Fragmentation approach to the point-island model with hindered aggregation: Accessing the barrier energy

Diego Luis González,[1,2,*] Alberto Pimpinelli,[3,2,†] and T. L. Einstein[2,4,‡]

[1]*Departamento de Física, Universidad del Valle, A.A. 25360, Cali, Colombia*
[2]*Department of Physics, University of Maryland, College Park, Maryland 20742-4111, USA*
[3]*Smalley-Curl Institute & Materials Science and Nanoengineering Department, Rice University, Houston, Texas 77005, USA*
[4]*CMTC, University of Maryland, College Park, Maryland 20742-4111, USA*

We study the effect of hindered aggregation on the island formation process in a one- (1D) and two-dimensional (2D) point-island model for epitaxial growth with arbitrary critical nucleus size i. In our model, the attachment of monomers to preexisting islands is hindered by an additional attachment barrier, characterized by length l_a. For $l_a = 0$ the islands behave as perfect sinks while for $l_a \to \infty$ they behave as reflecting boundaries. For intermediate values of l_a, the system exhibits a crossover between two different kinds of processes, diffusion-limited aggregation and attachment-limited aggregation. We calculate the growth exponents of the density of islands and monomers for the low coverage and aggregation regimes. The capture-zone (CZ) distributions are also calculated for different values of i and l_a. In order to obtain a good spatial description of the nucleation process, we propose a fragmentation model, which is based on an approximate description of nucleation inside of the gaps for 1D and the CZs for 2D. In both cases, the nucleation is described by using two different physically rooted probabilities, which are related with the microscopic parameters of the model (i and l_a). We test our analytical model with extensive numerical simulations and previously established results. The proposed model describes excellently the statistical behavior of the system for arbitrary values of l_a and $i = 1, 2,$ and 3.

I. INTRODUCTION

Growth processes provide interesting nonequilibrium phenomena, which have been the subject of several studies in recent years. It warrants emphasizing that the importance of growth processes goes beyond fundamental research. For example, controlling the atomistic mechanisms involved in thin-film growth is crucial in the production of nano- and microelectronic devices [1].

Typically, every growth process requires mass transport, nucleation, and aggregation. In the conceptually simplest implementation, thin-film growth on a substrate under vacuum, mass transport amounts to surface diffusion over the substrate. Considering homogeneous nucleation on a defect-free surface, aggregation happens through the attachment of the growth units—the diffusing atoms or molecules, that we will call monomers henceforth—to the clusters that have nucleated.

One of the characteristics of thin-film growth is that monomers are continuously—and randomly—deposited onto the substrate either from a beam or a vapor. Nucleation then takes place all over the substrate in such a way that a typical length scale—the average distance $\mathcal{L}$ between nuclei—can be defined. If we call D the monomer diffusion coefficient, monomers spend on average a time $\mathcal{L}^2/D$ diffusing between clusters. In many situations, attachment to a growing cluster simply requires that a diffusing monomer hops to a site adjacent to the cluster and forms a bond with it. In other situations, more complicated processes may be required, such as a chemical reaction, or a conformational change in the

attaching monomer. Subsuming all these processes into an additional activation barrier, one can define an "attachment rate" $1/\tau_a$. Then, aggregation is either limited by diffusion if $D/\mathcal{L}^2 \ll 1/\tau_a$ or by attachment in the opposite limit. The two regimes can thus be called diffusion-limited aggregation (DLA) and attachment-limited aggregation (ALA) [2–5].

In the DLA regime, attachment can be assumed to be instantaneous, since τ_a vanishes compared to the diffusion timescale $\mathcal{L}^2/D$. As mentioned above, in certain systems attachment to a cluster may be slowed down as though an additional energy barrier were present. This barrier might be due to strain, whose paradigmatic example is nucleation and growth of two-dimensional (2D) Ge islands on a Pb overlayer covering a Si(111) surface [6–9]. Attachment barriers might also be used to model the functioning of a catalyst, as in the case of graphene on metals [10–13] and oxides [14]. On metals, individual graphene islands spread at a constant rate, implying that their growth is controlled by the attachment rate of carbon to the islands edges. Since carbon comes from cracking a precursor in a reaction catalyzed by the metal, this particular kind of ALA process is often classified as reaction-limited aggregation (RLA). Finally, nucleation hindered by attachment barriers has been observed in metal (111) homoepitaxial systems [15,16] and for Fe deposition on graphene [17].

Depending on experimental conditions, both DLA and ALA can be observed in the same system. A crossover between DLA and ALA has been suggested in 3D colloidal systems [18,19] as well as in organic thin-film deposition [20,21]. (However, as proposed in Ref. [22], in organic systems the crossover may be due to other mechanisms than ALA.)

Initial studies in thin-film nucleation, both theoretical [3,23–28] and experimental [29–32], focused on the scaling behavior of the average cluster density, N, as a function of the deposition rate F. Theory predicted that $N \sim F^{\alpha}$, with a

---

*diego.luis.gonzalez@correounivalle.edu.co
†ap19@rice.edu
‡einstein@umd.edu

"growth exponent" α, which depends only on the size i of the critical nucleus and on the aggregation regime. Later on, the distributions of the cluster sizes, or island-size distributions (ISD), were investigated by using semiempirical expressions obtained by fitting numerical results from kinetic Monte Carlo (kMC) simulations [23,24,33]. Additionally, exact, though implicit, expressions requiring as input the size-dependence of the capture kernels were found [34,35]. Most of the studies about the ISD focus on growth in the DLA regime; however, recently the exact scaling form for the ISD in the ALA regime was obtained [36].

More recently, both theory and experiments have focused on another feature of the aggregation process, the so-called capture-zone distribution (CZD). (See Ref. [37] for reviews and Ref. [38] for recent results.) The CZ is the region of the substrate that is closer to the given aggregate in its interior than to any other aggregate. Thus, monomers deposited within a capture zone diffuse with the highest likelihood to that aggregate. They are essentially equivalent to Voronoi polygons determined by the centers of mass of the aggregates.

The functional forms of the CZD are not explicitly known in the experimentally relevant case of a 2D substrate, but two of the present authors (PE) have conjectured that the CZD can be approximated—at least in the experimentally important region near the central peak, away from the tails—by a generalization of the simple analytic expression known as the "Wigner surmise" [39,40]. This is a one-parameter family of functions, whose parameter β has been conjectured to be related to the critical nucleus size i and to the growth exponent α through $\beta = i/\alpha$ [21,39].

This conjecture has stimulated numerical work in 2D, as well as analytical studies on 1D model, which are amenable, if not to exact solutions, at least to detailed and controlled approximations.

Up to now, most theoretical investigations have been limited to DLA growth. Of the few studies considering the ALA regime, arguably the most prominent for 2D islands is Ref. [25]; more recently, Ref. [36] presents significant results on point islands. In the present paper, we report the first detailed analysis of a 1D model, which exhibits a crossover between DLA and ALA. We investigate the model using numerical kMC simulations, rate equations, and by computing analytically the CZD. We also study the "gap length distribution" (GLD), the distribution of the distances between aggregates. The ideas used in the 1D model are extended to describe growth on 2D systems. This situation is experimentally more relevant than the 1D case but is also more complex and does not allow the explicit calculation of many quantities [6–14].

The model presented here is meant as a minimal model, from which we can learn general properties of systems that exhibit a crossover between different nucleation regimes. Attachment-limited aggregation is obtained through an additional energy barrier, ϵ_a, lowering the attachment rate of monomers diffusing on the substrate toward a cluster edge. The various scaling regimes are studied in the framework of rate equations for monomers, subcritical, critical, and stable clusters. The detailed behavior of the system is investigated by solving numerically the fragmentation equation for the GLD in the framework of the so-called "point-island model," which is

described below. The CZD and the GLD are computed and then compared with an analytic—though approximate—treatment. Investigation of the CZD, in particular, are motivated not only for intrinsic theoretical interest but also because of their usefulness for real systems of technological relevance [22,37,41]. Moreover, the intermediate, crossover region has a rich and complex behavior.

As expected from Refs. [25,36], we found that the presence of an attachment barrier, ϵ_a, associated with the hindered aggregation process changes the growth exponents of the densities of islands and monomers. Additionally, ϵ_a modifies the GLD and CZD. This dependence, in principle, allows us to determine the barrier from experimental data. The model proposed in this paper is probably the simplest to implement numerically and, therefore, is an excellent testing ground that can be used to improve the analysis of experimental data.

II. MODEL DESCRIPTION

In epitaxial growth, monomers are deposited onto a substrate at a constant rate F; the temperature T of the substrate is usually selected in such a way that the evaporation of deposited monomers can be neglected. As usual, the critical nucleus size i is defined as the size of the largest unstable island. This means that the decay time of a stable island would be longer than the typical time that a monomer requires to become attached to an island. Note that the critical island size depends on temperature. An island with a certain number of monomers that is stable at some temperature may become unstable at a higher temperature.

In the proposed model, the monomers diffuse (with diffusion constant D) until they are captured by an island. Only the islands consisting of $i + 1$ or more monomers are completely stable. Islands smaller than $i + 1$ are unstable, i.e., the monomers belonging to such islands can diffuse away with diffusion constant D. For the sake of simplicity, we adopt the point-island model, where the size of an island is just the number of monomers that have attached to it but all are on the same lattice site; for more information, see Refs. [23,28,33,35,42–49].

In our growth model, monomers must hop onto an already occupied site in order to be incorporated. If the occupied site is a stable island, the diffusion process is hindered by an additional attachment barrier ϵ_a, which reduces the diffusion constant to D'. The associated characteristic length $l_a = \exp(\epsilon_a/k_B T) - 1$ is usually defined to measure the asymmetry between D and D' [50,51]. One can show that D and D' are related by $D/D' = l_a + 1$ [52]. This diffusion model implies that the ratio between the probability P_S to move the monomer to a stable island and the probability P_U to a site with fewer than $i + 1$ monomers is given by $P_U/P_S = \exp(\epsilon_a/k_B T)$. Thus, the probability to move to a stable island is given by $P_S = 1/[n_S + (2d - n_S)\exp(\epsilon_a/k_B T)]$, where n_S is the number of stable islands that are next neighbors of the monomer and d is the dimension of the system. Consequently, $P_U = 1/[n_S \exp(-\epsilon_a/k_B T) + (2d - n_S)]$. The assumption that the extra barrier only acts when monomers attach to a stable island implies that nucleation is independent of l_a. One can justify the alternative assumption that an attachment barrier also exists for unstable clusters [36].

The evolution of this system is frequently described in terms of the coverage $\theta = F t$, where t is the time. Since we neglect the evaporation of monomers previously deposited, θ is the number of monomers on the substrate. Two important quantities commonly used to describe the time evolution of the point-island model are the total density of free (diffusing) monomers, N_1, and the density of islands with size j, N_j. On the other hand, for 1D we define the spacing distribution functions, $\hat{p}^{(n)}(\mathcal{L})d\mathcal{L}$ as the probability that for an island at the origin there is another island at a distance between $\mathcal{L}$ and $\mathcal{L} + d\mathcal{L}$, with the condition that there are n additional islands inside the gap between them. The structure of the point-island system is usually described through the gap length distribution function $\hat{p}^{(0)}(\mathcal{L})$ and the capture zone distribution $\hat{P}(\mathcal{L}) = 2\hat{p}^{(1)}(2\mathcal{L})$ [42]. In a 1D system, the capture zone of an island is simply the distance between the midpoints of the gaps to the left and to the right of the island [23,35,42]. The scaled spacing is $\ell = \mathcal{L}/\langle \mathcal{L} \rangle$, with $\langle \mathcal{L} \rangle$ the average of $\mathcal{L}$. Then, the scaled spacing distributions are given by

$$p^{(n)}(\ell) = \langle \mathcal{L} \rangle \hat{p}^{(n)}(\ell \langle \mathcal{L} \rangle) \quad \text{and} \quad P(\ell) = 2p^{(1)}(2\ell). \quad (1)$$

In the 2D case, the substrate is not divided into gaps, and the structure formed by the islands is more complex than that in 1D. Instead of the gaps, the Voronoi cell or capture zone (CZ) of an island is defined by all the points on the substrate that are closer to the island than to any other island on the substrate.

III. RATE EQUATIONS

The time evolution of both the total density of [stable] islands $N = \sum_{j>i} N_j$ and of free monomers N_1 can be studied by standard rate equations in the mean-field (MF) approximation [27]. From the Appendix, N_1 and N obey

$$\frac{dN_1}{d\theta} = 1 - (i+1)\sigma_u \frac{D}{F} N_1^{i+1} - \frac{D}{F}\sigma_s N_1 N \quad (2)$$

and

$$\frac{dN}{d\theta} = \sigma_u \frac{D}{F} N_1^{i+1}, \quad (3)$$

respectively. The first term on the right side on Eq. (2) represents deposition of monomers in units of F, the second one the nucleation of new islands, and the last one relates to the capture of monomers by preexisting islands. As usual [23,46], σ_u is the capture coefficient (or "kernel") for critical islands, while σ_s is the capture kernel for stable islands. In general, σ_u is a function of temperature but also of the critical nucleus size i. However, in our point-island model the bond energy inside an unstable island vanishes, and it is effectively infinite inside a stable island. As a consequence, σ_u is independent of i and can be chosen constant.

There is, however, a complication. The nucleation process $(i+1)A \longrightarrow I$, where A is an adatom and I an island, has an upper critical dimension $d_c = 2/i$ [3]. Consequently, for a 1D system mean-field theory breaks down when $i = 1$. As we will recall below, one knows how to include corrections through the capture kernel σ_u. When $i = 2$, there will be logarithmic corrections [3] that can be neglected for our purposes. When $i > 2$, σ_u can in our case be assumed to be a constant, as discussed above. For a 2D system, σ_u is coverage independent

(neglecting logarithmic corrections). The aggregation process $A + I \rightarrow I$ has $d_c = \infty$; therefore, σ_s is a function of time for all values of i. Note that the dimensional dependence of Eqs. (2) and (3) is contained in the capture kernels.

The different behaviors can be characterized in terms of the density of islands N as a function of the coverage, θ (or equivalently the deposition rate F).

A. Growth exponents in 1D

From classical nucleation theory for the aggregation regime, if nucleation and aggregation are diffusion limited, $N \propto \theta^\beta$, where $\beta = 1/4$ for $i = 1$ and $\beta = 1/(2i+3)$ for $i \geqslant 2$ [3]. We derive the corresponding scaling relations for the case of attachment-limited aggregation.

In the low-coverage, L, regime, the density of free monomers is much larger than that of islands ($N_1 \gg N$). In this regime, Eq. (2) reduces to $dN_1/d\theta \approx 1$, and the density of monomers is given by $N_1 \approx \theta$. To determine the density of islands, it is necessary to calculate σ_u. The case $i = 1$ and $l_a = 0$ was studied in Ref. [46], where σ_u was calculated by estimating the density of monomers at a distance x from a given monomer, $n_1(x)$, in the aggregation regime. From $n_1(x)$, it is possible to calculate the incoming flux to the monomer, $2 D dn_1(x)/dx|_{x=0}$, which by definition is also given by $\sigma_u D N_1$. This process leads to

$$\sigma_u = \left(\frac{4F}{D N_1}\right)^{\frac{1}{2}}. \quad (4)$$

Even though Eq. (4) was calculated by using high-coverage arguments, Amar *et al.* [46] found that it is adequate even in the L regime.

This result also applies for $i = 1$ and arbitrary attachment barriers, because in this case the predominant process is also island formation, which, given our assumptions, does not depend on l_a. From Eqs. (3) and (4) it is easy to find

$$N \approx \frac{4}{5}\left(\frac{D}{F}\right)^{\frac{1}{2}} \theta^{\frac{5}{2}}. \quad (5)$$

For $i > 1$, σ_u can be replaced by a constant (σ_u^L), which depends on neither D/F nor l_a; see Ref. [53]. For $i = 2$ there are logarithmic corrections, which we neglect. Then, for any value of l_a, N behaves as

$$N \approx \frac{1}{i+2}\sigma_u^L \frac{D}{F}\theta^{i+2}. \quad (6)$$

Consistent with our assumption, in the L regime there is no dependence on l_a. Numerical results (not shown) from kinetic Monte Carlo (kMC) simulations of a 1D point-island model support this statement: for low θ the behavior of N and N_1 is the same for $l_a = 0$ and $l_a = 250$.

In contrast to the L regime, the aggregation, A, regime depends strongly on l_a. In this regime, the densities satisfy $N \gg N_1$ and $dN_1/d\theta \ll 1$ because the dominant process is the attachment of monomers to preexisting stable islands. Thus, Eq. (2) can be written as

$$1 - \frac{D}{F}\sigma_s N_1 N \approx 0; \quad (7)$$

consequently, $N_1 \approx (D \sigma_s N/F)^{-1}$. Inserting the latter in Eq. (3) yields

$$\frac{dN}{d\theta} = \sigma_u^A \left(\frac{F}{D}\right)^i (\sigma_s N)^{-(i+1)}, \qquad (8)$$

where σ_u^A is the capture kernel for unstable clusters in the aggregation regime. We now extend the method of Ref. [23] to calculate σ_s for arbitrary l_a and i. In the continuum limit, the stationary density of diffusing monomers at position x inside a gap with length $\mathcal{L}$, $n_1(x,\mathcal{L})$, is given by the solution of

$$D \frac{d^2 n_1(x,\mathcal{L})}{dx^2} + F = 0, \qquad (9)$$

with $l_a d n_1(x,\mathcal{L})/dx|_{x=0} = n_1(0,\mathcal{L})$ and $l_a d n_1(x,\mathcal{L})/dx|_{x=\mathcal{L}} = -n_1(\mathcal{L},\mathcal{L})$. Note that for $l_a = 0$ the stable islands are perfect traps, while for $l_a \to \infty$ they behave as reflecting boundaries. The solution of Eq. (9) can be found easily:

$$n_1(x,\mathcal{L}) = \frac{F}{2D}\left(l_a \mathcal{L} + \mathcal{L} x - x^2\right). \qquad (10)$$

The total flux of monomers into a stable island is given by

$$\sigma_s = \frac{1}{N_1}\left(\frac{dn_1(x,\mathcal{L})}{dx}\bigg|_{x=0^+} - \frac{dn_1(x,\mathcal{L})}{dx}\bigg|_{x=0^-}\right), \qquad (11)$$

where $dn_1(x,\mathcal{L})/dx|_{x=0^{+[-]}}$ represents the derivative of $n_1(x,\mathcal{L})$ at the right [left] boundary of the island. By using Eq. (10), we find

$$\sigma_s = \frac{F \mathcal{L}^{CZ}}{N_1 D}, \qquad (12)$$

where $\mathcal{L}^{CZ} = (\mathcal{L}^+ + \mathcal{L}^-)/2$ is the length of the island's capture zone (CZ), $\mathcal{L}^+$ and $\mathcal{L}^-$ being the lengths of the gaps to the right and left of the island, respectively. The total number of monomers inside a gap with length $\mathcal{L}$ is then

$$n_{\mathcal{L}} = \int_0^{\mathcal{L}} dx\, n_1(x,\mathcal{L}) = \frac{l_a \mathcal{L}^2 F}{2D} + \frac{F \mathcal{L}^3}{12 D}, \qquad (13)$$

implying that the total number of monomers inside a gap for $l_a \gg 1$ is larger than that same number for $l_a \ll 1$, by a factor $6 l_a/\mathcal{L} \gg 1$. The total density of free monomers can be calculated from

$$N_1 = N \int dy\, n_y\, p^{(0)}(y), \qquad (14)$$

which implies

$$N_1 N = \frac{F l_a \langle \ell_g^2 \rangle}{2D} + \frac{F \langle \ell_g^3 \rangle}{12 D N}, \qquad (15)$$

where $\ell_g = N\mathcal{L}$ is the scaled length of the gap and $\langle \cdots \rangle$ is the average taken over the ensemble of islands. Defining the scaled length of a capture zone $\ell_{CZ} = N\mathcal{L}^{CZ}$, averaging Eq. (12) over all islands and using Eq. (15), it follows that in the case of vanishing barriers, $l_a = 0$,

$$\sigma_s = 12 \langle \ell_{cz} \rangle N / \langle \ell_g^3 \rangle = \mathfrak{a}_1 N, \qquad (16)$$

with $\langle s_{cz} \rangle = 1$ and $\mathfrak{a}_1 \approx 7.5$. Similarly, in the limit of strong barriers, $l_a \gg 1$,

$$\sigma_s = 2 \langle \ell_{cz} \rangle / l_a \langle \ell_g^2 \rangle = \mathfrak{b}_1 / l_a, \qquad (17)$$

with $\mathfrak{b}_1 \approx 1.9$.

For $i = 1$, σ_u is then given by Eq. (4) while σ_s is given by Eq. (16) or (17) depending on the value of l_a. Accordingly, in the limit $l_a \ll 1$, N_1 and N take the form

$$N_1(\theta) \approx \frac{\theta^{-\frac{1}{2}} F^{\frac{1}{2}}}{2^{\frac{3}{2}} D^{\frac{1}{2}} \mathfrak{a}_1^{\frac{1}{4}}} \quad \text{and} \quad N(\theta) \approx \left(\frac{8\,\theta\, F}{D\, \mathfrak{a}_1^{\frac{3}{2}}}\right)^{\frac{1}{4}}, \qquad (18)$$

respectively. Last expression for N was obtained previously in Ref. [3]. On the other hand, in the limit $l_a \gg 1$, σ_s is given by Eq. (17); hence, integrating we find

$$N(\theta) \approx \left[\frac{3\,\sigma_u^A F\,\theta\,l_a^2}{D\,\mathfrak{b}_1^2}\right]^{\frac{1}{3}} \quad \text{and} \quad N_1(\theta) \approx \left(\frac{l_a F^2}{3\,D^2\,\mathfrak{b}_1\,\sigma_u^A\,\theta}\right)^{\frac{1}{3}}. \qquad (19)$$

The densities in the case $i \geqslant 2$ with vanishing barriers can be calculated similarly by taking $\sigma_u = \sigma_u^A$ as a constant and assuming that $\sigma_s = \mathfrak{a}_i N$ has the same form as Eq. (16). Thus, after integration it is found

$$N(\theta) \approx \left(\frac{\mathfrak{c}_1 F^i\,\theta}{D^i\,\mathfrak{a}_i^{i+1}}\right)^{\frac{1}{2i+3}} \quad \text{and} \quad N_1(\theta) \approx \left(\frac{(F/D)^{3/2}}{\mathfrak{c}_1\,\theta\,\mathfrak{a}_i^{1/2}}\right)^{\frac{2}{2i+3}}, \qquad (20)$$

where $\mathfrak{c}_1 = (2i+3)\sigma_u^A$.

Finally, in the case $i \geqslant 2$ and strong barriers, we take $\sigma_s = \mathfrak{b}_i/l_a$ and $\sigma_u = \sigma_u^A$. After integration, we obtain

$$N(\theta) \approx \left(\frac{\mathfrak{c}_2 F^i\,\theta\,l_a^{i+1}}{D^i\,\mathfrak{b}_i^{i+1}}\right)^{\frac{1}{i+2}} \quad \text{and} \quad N_1(\theta) \approx \left(\frac{l_a F^2}{D^2 \mathfrak{b}_i\,\theta}\right)^{\frac{1}{i+2}}, \qquad (21)$$

with $\mathfrak{c}_2 = (i+2)\sigma_u^A$.

The quantities $\mathfrak{a}_i$ and $\mathfrak{b}_i$ are numbers defined analogously to $\mathfrak{a}_1$ and $\mathfrak{b}_1$, respectively. They depend on i through the i-dependence of the probability distributions used in the averaging process.

For $i = 1$, the crossover coverage θ_c between the L and the A regime can be found for $l_a \ll 1$ and $l_a \gg 1$ by equating Eqs. (5) to (18) [$l_a \ll 1$] and Eqs. (5) to (19) [$l_a \gg 1$], respectively. It is straightforward to compute the crossover coverage θ_c for $i \geqslant 2$ by an equivalent procedure. The results are shown in Table I.

The corresponding island densities scale as

$$N_c(\theta_c) \sim \left(\frac{F}{D}\right)^{\frac{i+1}{2i+5}} \quad \text{and} \quad N_c(\theta_c) \sim l_a^{\frac{i+2}{i+3}}\left(\frac{F}{D}\right)^{\frac{i+1}{i+3}}, \qquad (22)$$

for $l_a \ll 1$ and $l_a \gg 1$, respectively.

TABLE I. Crossover coverage θ_c for different values of i in the regime of weak and strong attachment barriers. In all cases there are numerical factors of order unity.

θ_c	$l_a \ll 1$	$l_a \gg 1$
$i = 1$	$(F/D)^{1/3}$	$l_a^{4/13}(F/D)^{5/13}$
$i \geqslant 2$	$(F/D)^{3/(2i+5)}$	$[l_a (F/D)^2]^{1/(i+3)}$

Therefore, the crossover coverage and the corresponding island density also increase with l_a: as a matter of fact, when $l_a \to \infty$ attachment is completely suppressed, and the aggregation regime disappears altogether. However, for $i = 1$ and typical values of $D/F \approx 10^6$, one would need $l_a \approx 10^8$ in order for $\theta_c = 1$.

For large barriers, there is a region in the crossover where the island density is proportional to the coverage, as follows. At early deposition times (small coverage), aggregation is negligible:

$$\sigma_s D' N_1 N(\theta) \ll \sigma_u (i + 1) D N_1^{i+1}. \qquad (23)$$

In this regime, deposition is balanced by nucleation,

$$1 - (i + 1)\sigma_u \frac{D}{F} N_1^{i+1} \approx 0; \qquad (24)$$

then, from Eq. (3), the density of monomers can be written as

$$N_1 \approx \left[\frac{F}{(i+1)\sigma_u D} \right]^{1/(i+1)}. \qquad (25)$$

Consequently, the island density satisfies

$$N \approx \sigma_u N_1^{i+1} \frac{D}{F} \theta = \frac{\theta}{i+1}. \qquad (26)$$

A summary of the scaling exponents of the densities of monomers and islands, $N_1 \propto (F/D)^{\alpha_1} \theta^{\beta_1}$ and $N \propto (F/D)^{\alpha} \theta^{\beta}$ in the A regimes can be seen in Table II. To evaluate the exponents we used Eqs. (18) to (21), and we assumed that σ_u^A and $\mathfrak{b}_i$ depend on neither D/F nor l_a.

Figure 1 illustrates the behavior of N_1 and N in kMC simulations of the point-island model, as a function of the coverage for $D/F = 5 \times 10^6$. The panels exhibit log-log plots of the free monomers (left) and island density (right) for a large but finite attachment barrier. Straight lines are drawn in each panel according to the power-law exponents predicted by the rate equation analysis for the corresponding values of l_a and of the critical nuclei. Crossovers between the L and A regimes can be identified as the coverages at which these straight lines cross each other, for each value of i. Excellent agreement was

TABLE II. In the aggregation regime we define the exponents according to $N \propto (D/F)^{-\alpha}\theta^{\beta}$ and $N_1 \propto (D/F)^{-\alpha_1}\theta^{\beta_1}$. *For $l_a \ll \langle s \rangle$, the entries for general i do not apply for $i = 1$.

Exp.	i		$i = 1$		$i = 2$		$i = 3$	
$l_a/\langle s \rangle$:	$\ll 1^*$	$\gg 1$	$\ll 1$	$\gg 1$	$\ll 1$	$\gg 1$	$\ll 1$	$\gg 1$
α	$\frac{i}{2i+3}$	$\frac{i}{i+2}$	1/4	1/3	2/7	1/2	1/3	3/5
α_1	$\frac{3}{2i+3}$	$\frac{2}{i+2}$	1/2	2/3	3/7	1/2	1/3	2/5
β	$\frac{1}{2i+3}$	$\frac{1}{i+2}$	1/4	1/3	1/7	1/4	1/9	1/5
β_1	$\frac{-2}{2i+3}$	$\frac{-1}{i+2}$	$-1/2$	$-1/3$	$-2/7$	$-1/4$	$-2/9$	$-1/5$
Eqs.			(18)	(19)	(20)	(21)	(20)	(21)

also found for the case of vanishing attachment barriers (not shown).

As expected from Eqs. (2) and (3), in the L regime the exponents do not depend on l_a. This is a consequence of our assumption that nucleation is independent of l_a. In the A regime, for a given coverage, N increases with l_a because each stable island acts as reflecting boundary, favoring the nucleation of new stable islands. In the quite unphysical limit $l_a \to \infty$, islands can only nucleate but cannot grow in size beyond $i + 1$.

The validity of Eq. (26) was also corroborated by numerical simulations (not shown).

B. Growth exponents in 2D

For the 2D case, the growth exponents can be calculated following an analogous procedure to that used in the 1D case. However, the 2D case is intrinsically simpler because, if we neglect logarithmic corrections, the capture coefficient σ_u can be taken as a coverage-independent constant for all values of i. From Eqs. (2) and (3), the evolution of N and N_1 in the L regime is given by $N_1 \approx \theta$ and

$$N \approx \frac{D\sigma_u}{F(i+2)} \theta^{i+2}. \qquad (27)$$

By assumption, the early-time evolution is independent of the aggregation barrier.

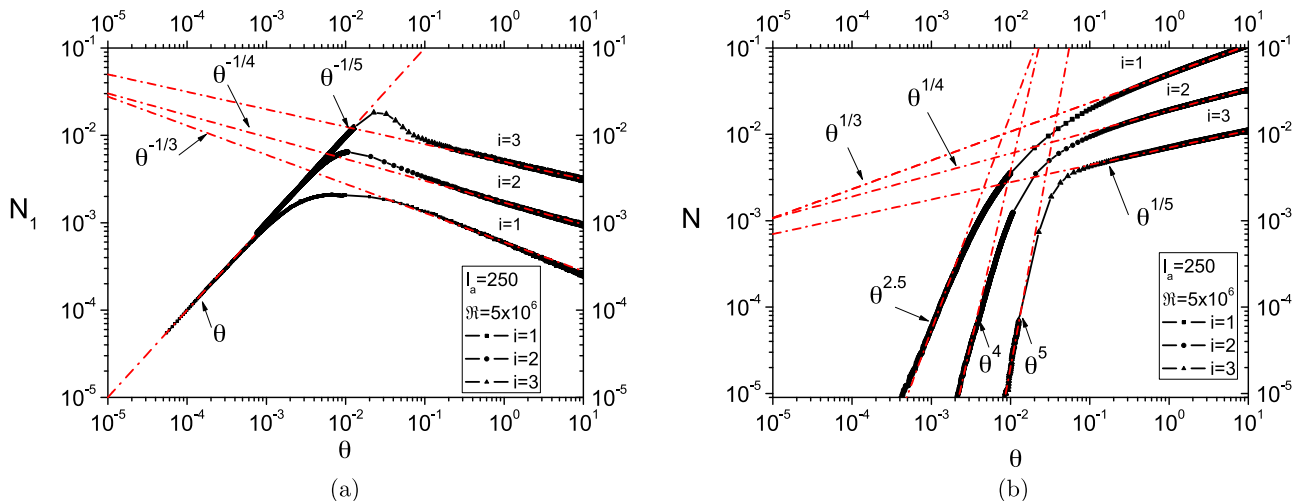
FIG. 1. Time evolution of (a) N_1 and (b) N for $D/F = 5 \times 10^6$ and large but finite attachment barriers $l_a = 250$. Three different values of i were considered: 1, 2, and 3. See text for discussion.

For the A regime with zero and weak barriers, Eq. (7) is satisfied, leading to [44]

$$N_1 \propto \left(\frac{F}{D}\right)^{2/(i+2)} \theta^{-1/(i+2)} \tag{28}$$

and

$$N \propto \left(\frac{F}{D}\right)^{i/(i+2)} \theta^{1/(i+2)}. \tag{29}$$

For strong barriers the monomers need many attempts to be incorporated into a stable islands, favoring the formation of new islands. As in the 1D case, at early deposition times (small coverage), aggregation is negligible and deposition is balanced by nucleation, implying $N \approx \frac{\theta}{i+1}$. This regime lasts until Eq. (23) breaks down, which happens at an i-dependent critical coverage $\theta_c^{(i)}$ obeying $\sigma_s N_1 N(\theta_c^{(i)}) \approx \sigma_u(i+1)(l_a+1)N_1^{i+1}$, so that using Eqs. (25) and (26), and letting $\sigma_s \approx \sigma_u \approx 1$, as well as $D/D' = l_a + 1$, yields

$$\theta_c^{(i)} \approx (l_a+1)(i+1)^{(i+2)/(i+1)}\left(\frac{F}{D}\right)^{i/(i+1)}. \tag{30}$$

We can estimate $\theta_c^{(i)}$ for the values $D/F = 5 \times 10^6$, $l_a = 250$ used in our simulations; we find $\theta_c^{(1)} \approx 0.71$ and $\theta_c^{(2)} \approx 0.11$ for $i = 1$ and 2, respectively. This implies, at least qualitatively (since we set $\sigma_s/\sigma_u = 1$), that the regime, in which the island density is proportional to the coverage, becomes harder to observe as the critical nucleus size i increases, for a given value of l_a. In other words, we predict that the same θ_c will be observed for $i = 1$ and 2 when l_a is approximately seven times larger for $i = 2$ than for $i = 1$, with our choice of parameters. This prediction is well borne out by our simulations, as discussed below.

The condition $1 > \theta > \theta_c^{(i)}$ defines the aggregation (A) regime. In this regime, the relation

$$1 - \frac{D}{F}\sigma_s N_1 N \approx 0 \tag{31}$$

holds. However, in 2D the attachment coefficient σ_s depends on both l_a and N if aggregation is attachment limited. Indeed, σ_s acquires a dependence on the length of the island perimeter, which in turn scales like $\mathcal{L}_N = 1/\sqrt{N}$ (since in the aggregation regime the average distance between islands $\mathcal{L}_N$ is the only relevant length scale.) As a consequence, both vanishingly small and very large barriers can be described by letting

$$\sigma_s = \sigma_s^0\left(1 + \frac{l_a}{\mathcal{L}_N}\right). \tag{32}$$

The free monomer density N_1 takes the form

$$N_1 \approx \frac{F}{D\sigma_s^0 N}\left(1 + \frac{l_a}{\mathcal{L}_N}\right), \tag{33}$$

where again $\mathcal{L}_N = 1/\sqrt{N}$. The second term in the parenthesis on the right side of Eq. (33) describes the action of the barrier at the perimeter of an island of typical linear size $R \sim \mathcal{L}_N$. The latter holds in the aggregation regime. Inserting Eq. (33) into Eq. (3) yields

$$N \sim \left(\frac{F}{D}\right)^{i/(i+2)} \tag{34}$$

for $l_a \ll \mathcal{L}_N$, and

$$N \sim \left(\frac{F}{D}\right)^{2i/(i+3)} \tag{35}$$

for $l_a \gg \mathcal{L}_N$.

Equation (33) does not hold, however, for point islands, since the latter have, by definition, a boundary of vanishing extension. Equation (33) becomes in this case $N_1 \approx \frac{F}{DN}(1 + l_a)$, and the same growth exponent as in Eq. (34) is found for any value of the attachment barrier.

The predicted power-law behavior of N_1 and N is confirmed by our kMC simulations for $i = 1$, 2, and 3 (not shown) and for various attachment barriers. Our results agree with those reported in Ref. [36]. The point-island model turns out to be not appropriate to describe the crossover between DLA and ALA in 2D, if one only considers the behavior of the island density as a function of F. We will show, however, that the CZD strongly depends on the attachment barrier in 1D and 2D, even for the point-island model.

IV. SPATIAL DESCRIPTION OF NUCLEATION

A. Fragmentation model in 1D

Both the spacing (gap) distribution functions between islands $\hat{p}^{(0)}(\mathcal{L})$ and the capture-zone distribution $\hat{P}(\mathcal{L})$ have relevant physical information about the nucleation process. We restrict our studies to the aggregation regime, where there is a quasisteady state. A good description of the nucleation inside the gaps is required to calculate $\hat{p}^{(0)}(\mathcal{L})$ and $\hat{P}(\mathcal{L})$. Following Ref. [42], let $Q(x, \mathcal{L})$ be the joint probability density that a given new nucleation occurs at position x inside a gap of length $\mathcal{L}$. Of course, $x < \mathcal{L}$; otherwise, $Q(x, \mathcal{L}) = 0$. Let $q_x(x)$ be the probability density that a given nucleation occurs at position x inside a gap of any size. Then,

$$q_x(x) = \int_x^\infty d\mathcal{L}\, Q(x, \mathcal{L}). \tag{36}$$

Similarly, the probability density $q_{\mathcal{L}}(\mathcal{L})$ that a given nucleation occurs anywhere inside a gap of length $\mathcal{L}$ is given by

$$q_{\mathcal{L}}(\mathcal{L}) = \int_0^{\mathcal{L}} dx\, Q(x, \mathcal{L}). \tag{37}$$

Finally, the probability density that a nucleation occurs at position x in a gap of length $\mathcal{L}$ under the condition $\chi = x/\mathcal{L} < 1$ is

$$p^\chi(\chi) = \int_0^\infty d\mathcal{L}\, \mathcal{L}\, Q(\chi\mathcal{L}, \mathcal{L}). \tag{38}$$

Note that $p^\chi(\chi)$ can be interpreted as the average nucleation probability density over the system of islands. An analytical expression relates the gap-size distribution $p^{(0)}(\ell)$ and $Q(x, \mathcal{L})$:

$$\ell\frac{dp^{(0)}(\ell)}{d\ell} + 2\, p^{(0)}(\ell) = -q_{\mathcal{L}}(\ell) + 2\, q_x(\ell); \tag{39}$$

for additional information, see Refs. [23,42]. By using Eq. (39) and an approximation for $Q(x, \mathcal{L})$, one can calculate $p^{(0)}(\ell)$. Several analytical solutions for Eq. (39) with simple fragmentation kernels $p^\chi(\chi)$ can be found in Refs. [54,55]. In particular, it is well established that the left tail of

the distribution $p^{(0)}(\ell)$ depends on the fragmentation kernel $p^\chi(\chi)$, while the right tail depends on $q_\mathcal{L}(\ell)$. In Refs. [54–56] it was shown that for large ℓ,

$$p^{(0)}(\ell) \propto \ell^{p^\chi(1)-2} e^{-c\,\ell^\gamma}, \tag{40}$$

for some constant $c > 0$, and γ is given by $\ell^\gamma = q_\mathcal{L}(\ell)/p^{(0)}(\ell)$. On the other hand, for small ℓ,

$$p^{(0)}(\ell) \propto \ell^\mu, \tag{41}$$

with $p^\chi(\chi) = \chi^\mu(a_1 + a_2\chi + \cdots)$.

However, an integrodifferential equation like Eq. (39) is generally hard to solve analytically or numerically. Nevertheless, Eq. (39) can be solved easily in a statistical way, even for complex functional forms of $p^\chi(\chi)$; see Refs. [23,42]. While Eq. (39) can also be solved using a self-consistent method [57], the statistical method allows one to determine directly all spacing-distribution functions, $p^{(n)}(\ell)$, defined in Sec. II.

In the spirit of Ref. [42], it is reasonable to propose

$$Q(x,\mathcal{L}) = \wp(x,\mathcal{L}) \frac{\omega(\mathcal{L})}{\Omega} p^{(0)}(\mathcal{L}), \tag{42}$$

where

$$\Omega = \int_0^\infty d\mathcal{L}\,\omega(\mathcal{L})\,p^{(0)}(\mathcal{L}), \tag{43}$$

and $\omega(\mathcal{L})$ is proportional to the rate of nucleation inside a gap of size $\mathcal{L}$, i.e., proportional to the number of nucleations inside a gap per unit time. On the other hand, $p^{(0)}(\mathcal{L})$ is the size distribution of the gaps and $\wp(x,\mathcal{L})$ is the probability of nucleation *inside* a single gap. In the fragmentation approach, the information about the nucleation process is contained in $\wp(x,\mathcal{L})$ and $\omega(\mathcal{L})$. We have chosen $\wp(x,\mathcal{L})$ and $\omega(\mathcal{L})$ as fundamental quantities to describe nucleation because they have been studied for different values of i and l_a; see Ref. [51]. The next section is devoted to the calculation of these quantities.

1. Mean field (uniform nucleation) approximation (MF)

In the MF approximation, the probability of nucleation at position x inside a gap with length $\mathcal{L}$, $\wp(x,\mathcal{L})$, is assumed—as in the Walton relation [58]—to be proportional to $n_1(x,\mathcal{L})^{i+1}$, with $n_1(x,\mathcal{L})$ given by Eq. (10) [23,42,56]:

$$\wp(x,\mathcal{L}) = \frac{n_1(x,\mathcal{L})^{i+1}}{\int_0^\mathcal{L} dx\,n_1(x,\mathcal{L})^{i+1}}, \tag{44}$$

with $i+1$ the minimum number of monomers required to form a stable island. Inserting $n_1(x,\mathcal{L})$ from Eq. (10), one can calculate the integral in Eq. (44) explicitly for arbitrary i and l_a,

$$\int_0^\mathcal{L} dx\,n_1(x,\mathcal{L})^{i+1} = [\mathcal{L}(4l_a+l)]^{\frac{3}{2}+i} F(b_1,b_2,b_3), \tag{45}$$

with

$$F(b_1,b_2,b_3) = \left(\mathrm{B}\left[\tfrac{1}{2}b_2,b_3,b_3\right] - \mathrm{B}\left[\tfrac{1}{2}b_1,b_3,b_3\right]\right), \tag{46}$$

where $\mathrm{B}[\cdot,\cdot,\cdot]$ is the incomplete beta function, $b_{1,2} = 1 \mp (1+4l_a/\mathcal{L})^{-1/2}$ and $b_3 = 2+i$. In the simplest case, $i = 1$,

$\wp(x,\mathcal{L})$ takes the form

$$\wp(x,\mathcal{L}) = \frac{30[x^2 - \mathcal{L}(l_a+x)]^2}{\mathcal{L}^3(\mathcal{L}^2 + 10\,\mathcal{L}\,l_a + 30\,l_a^2)}. \tag{47}$$

Note that for $l_a = 0$, we recover the established result $\wp(x,\mathcal{L}) = 30(x^2 - \mathcal{L}\,x)^2/\mathcal{L}^5$ [23,42]. For the case $l_a \to \infty$, the dependence on x disappears, and $\wp(x,\mathcal{L}) = 1/\mathcal{L}$.

The total nucleation rate of a single gap with size $\mathcal{L}$, $\omega(\mathcal{L})$ is proportional to the integral in Eq. (45). After some algebra, we find that $\omega \propto \mathcal{L}^{2i+3}$ for $\mathcal{L} \gg l_a$, while $\omega \propto \mathcal{L}^{i+2}$ for $\mathcal{L} \ll l_a$. Additionally, for $i = 1$, using the integral in Eq. (45), $\omega(\mathcal{L})$ takes the form

$$\omega(\mathcal{L}) \propto \frac{D^2}{120F^2}\mathcal{L}^3(\mathcal{L}^2 + 10\,\mathcal{L}\,l_a + 30\,l_a^2). \tag{48}$$

Then, for zero barriers ($l_a = 0$), we recover the well-known result for $i = 1$, $\omega(\mathcal{L}) \propto \mathcal{L}^5$ [23,42]; for large barriers, $\omega(\mathcal{L}) \propto l_a^2 \mathcal{L}^3$. The attachment barrier increases the nucleation rate inside gaps.

2. Castellano and Politi approximation (CP)

In the Castellano-Politi (CP) approach, the unnormalized probability of nucleation at position n inside a gap with size $\mathcal{L}$, $\tilde\wp(n,\mathcal{L})$ is given by

$$\tilde\wp(n,\mathcal{L}) = \sum_{t=0}^\infty \Phi(n;t+1), \tag{49}$$

where $\Phi(n;t)$ is the probability of nucleation inside a gap at the position n and time t; see Refs. [51,59–61]. The total nucleation rate $\omega(\mathcal{L})$ inside a gap with size $\mathcal{L}$ can be calculated from Eq. (49):

$$\omega(\mathcal{L}) = F\,\mathcal{L}\left[\frac{1}{i!}\left(\frac{\tau_{\mathrm{res}}}{\tau_{\mathrm{dep}}}\right)^i\right]\sum_{n=1}^\mathcal{L} \tilde\wp(n,\mathcal{L}), \tag{50}$$

where $\tau_{\mathrm{res}} = \mathcal{L}/[(12D)(\mathcal{L} + 6l_a)]$ is the average time that a single monomer spends inside a gap and $\tau_{\mathrm{dep}} = 1/(F\mathcal{L})$ is the typical time between consecutive depositions. In Eq. (50), the factor $F\mathcal{L}$ represents the number of monomers arriving into the gap per unit time, the factor inside square braces is the probability to find i monomers at the time of the $(i+1)$th deposition and the last factor is the conditional nucleation probability given that there are $i+1$ monomers inside the gap; see Ref. [51]. CP [59–61] showed that in the limit of large gaps and for $i = 1$, $\omega(\mathcal{L}) \approx 0.4F^2\mathcal{L}^4/D$ for zero and weak barriers, $\omega(\mathcal{L}) \approx 0.5\,F^2\mathcal{L}^3\,l_a/D$ for strong but finite barriers, and $\omega(\mathcal{L}) = (F\mathcal{L})^{-1}$ for infinite barriers. For large values of l_a and arbitrary i, one can calculate the nucleation rate. Following Refs. [51,52], for large gaps, $\omega(\mathcal{L})$ can be written as

$$\omega(\mathcal{L}) \propto F^{i+1}l_a^i \mathcal{L}^{2i+1}. \tag{51}$$

In Ref. [51], $\omega(\mathcal{L})$ was calculated from Eq. (50) by solving Eq. (49) numerically. The results agree with the ones given by Eq. (51) in the limit of large l_a. In Table III we summarize the results, using the CP approach, for the exponent γ in $\omega(\mathcal{L}) \propto \mathcal{L}^\gamma$ presented in Ref. [51]. The results show that for $i \geqslant 3$, CP's approach gives the same γ values as the MF approximation, even for small or zero attachment barriers. In order to understand this result, we recall that the dynamics

TABLE III. Exponent γ of the nucleation rate in 1D in the CP and MF approximations [51]. The MF values of γ are $i + 2$ and $2i + 3$ for $l_a \gg \mathcal{L}$ and $\mathcal{L} \gg l_a$, respectively. For $\mathcal{L} \gg l_a$, CP and MF essentially coincide for $i \geqslant 2$ ($\gamma = 2i + 3$) with small discrepancies for $i = 2$. However, for $i = 1$ CP approach gives $\gamma = 4$, while MF gives $\gamma = 5$.

γ	$\mathcal{L} \gg l_a$		$\mathcal{L} \ll l_a$	
	CP	MF	CP ($2i+1$)	MF ($i+2$)
$i = 1$	4	5	3	3
$i = 2$	6.875	7	5	4
$i \geqslant 3$	$2i + 3$		$2i + 1$	$i + 2$

of $i + 1$ monomers in $d = 1$ can be interpreted as that of a single monomer in dimension $d = i + 1$. Some properties of random walks, such as recurrence, number of visited sites, etc., depend on d. The behavior of γ seems to be a consequence of this fact. The results shown on Table III suggest a critical dimension $d_c = 3$ ($i = 2$). In fact, the noninteger value of γ for $i = 2$ seems to be related to the typical logarithmic corrections that appear when the dimension of the system is equal to d_c.

As reported in Refs. [42,43], we anticipate corrections to these γ values. First of all, in our system we have an ensemble of gaps, and each gap has a nucleation rate that depends on its length. Second, the CP approach assumes that when the $(i + 1)$th monomer arrives, the average monomer density profile has reached its stationary state. This is not true for large gaps because they have faster nucleation than smaller ones. Consequently, the average monomer density profile does not have sufficient time to reach its stationary state given by Eq. (10).

3. Phenomenological model (PM)

In the MF approach, Eq. (42) is completely determined by Eqs. (44) and (45). The MF expressions give good results for arbitrary i and small values of l_a but fail for large values of the attachment barrier [42,59–61]. On the other hand, while Eq. (42) can be evaluated in CP's method by using Eqs. (49) and (50), there are no explicit expressions for $\wp(n, \mathcal{L})$ or $\omega(\mathcal{L})$ for general i and l_a. Hence, to make progress we adopt a simpler model, which uses some results from both the MF and CP approaches. First, the MF approximation suggests a polynomial approximation for $p^\chi(\chi)$. An advantage of this simplification is that solutions of Eq. (39) have been thoroughly studied for this kind of kernel; see Sec. 6 in Ref. [54]. For arbitrary values of i and l_a, it is generally reasonable to propose

$$p^\chi(\chi) = a_1 \chi + \cdots + a_{i+1} \chi^{i+1} + \cdots + a_{2(i+1)} \chi^{2(i+1)}, \tag{52}$$

where the a_k are unknown coefficients which depend on l_a and i. Taking into account the following properties of $p^\chi(\chi)$:

(1) $p^\chi(\chi) = p^\chi(1 - \chi)$ (symmetry),

(2) $\int_0^1 d\chi \, p^\chi(\chi) = 1$ (normalization)

minimizes the number of fitting parameters. A simple calculation shows that, for $l_a > 0$, there are just i fitting parameters in Eq. (52). Furthermore, for $l_a = 0$ and arbitrary i there are no fitting parameters, and $p^\chi(\chi)$ is equivalent to that

obtained from Eqs. (38) and (42) in the MF approach, $p^\chi(\chi) = a \chi^{i+1} (1 - \chi)^{i+1}$, with the constant a determined by the normalization condition. This implies that in Eq. (52) $a_j = 0$ for $j < i + 1$, while for $j \geqslant i + 1$ the a_j are binomial coefficients (times a); e.g., $p^\chi(\chi) = a(\chi^2 - 2\chi^3 + \chi^4)$ for $i = 1$.

Second, we propose

$$\omega(\mathcal{L}) \propto \mathcal{L}^\gamma \quad \text{with} \quad \gamma(\ell) = \begin{cases} \gamma_{\text{ex}} - 1, & \text{if } \ell > \ell_c, \\ \gamma_{\text{ex}}, & \text{if } \ell \leqslant \ell_c, \end{cases} \tag{53}$$

where γ_{ex} is an integer exponent close or equal to the one given by CP's method (as specified after Eq. (40)), and ℓ_c is a phenomenological critical scaled size for the gaps. Equation (53) captures the lower nucleation-rate exponent for large gaps. We used this approach successfully to describe the nucleation process for the case $i = 1$ and $l_a = 0$ [42]. In fact, the choice $\gamma = 4$ for $\ell < 1.7$ and $\gamma = 3$ for $\ell > 1.7$, with an appropriate description of $\wp(x, \mathcal{L})$, gives excellent results for both $p^{(0)}(\ell)$ and $P(\ell)$ [42]. Henceforth, we will refer to this approach, embodied in Eqs. (52) and (53), as the phenomenological model (PM).

B. Fragmentation model in 2D

The functional forms of the CZ distribution in the A regime, for arbitrary dimension and critical-nucleus size with $l_a = 0$, have been the subject of recent discussion and some controversy [35,39,40,62–64]. However, as far as we know, almost nothing has been said about the case of hindered aggregation ($l_a > 0$) [21]. The structure formed by the islands in 2D is more complex than that in 1D, thwarting analytical calculation of many quantities. In the 2D case it is necessary to describe the nucleation inside capture zones instead of nucleation inside gaps. Following Ref. [65], let $q^c(\mathcal{A})$ be the probability density to put a new center within a Voronoi cell having a scaled area $\mathcal{A}$ (i.e. area/$\langle$area$\rangle$). Following Eq. (53), we propose for the 2D case the analog of $\omega(\mathcal{L})$ for 1D,

$$q^c(\mathcal{A}) = \frac{\mathcal{A}^\phi}{\tilde{\mu}_\phi} P(\mathcal{A}), \tag{54}$$

where $\tilde{\mu}_\phi$ is the ϕth moment of $P(\mathcal{A})$. In Eq. (54) it is assumed that nucleation occurs inside capture zones rather than inside gaps, which are ill-defined in 2D. The exponent ϕ determines the large-$\mathcal{A}$ tail of the CZD [62]. For instance, $\phi = 1$ and $\phi = 2$ imply exponential and Gaussian decay, respectively. Additionally, $q^r(\mathbf{r}, \mathcal{A})$ is defined as the probability density that, for a particular cell with scaled size $\mathcal{A}$, the new center is located at a scaled position $\mathbf{r}$ with respect to the center of the preexisting cell. For simplicity, just the isotropic case is considered, inviting the introduction of the physically motivated exponent δ:

$$q^r(\mathbf{r}, \mathcal{A}) \sim r^\delta, \quad r \equiv |\mathbf{r}|. \tag{55}$$

However, the slope of the monomer density, $n_1(r)$, vanishes along the boundaries of the CZ. A simple way to accomplish this goal for the point-island model is to propose

$$q^r(\mathbf{r}, \mathcal{A}) \sim \begin{cases} r^\delta, & \text{if } 0 \leqslant r \leqslant \kappa R_c, \\ (\kappa R_c)^\delta, & \text{if } \kappa R_c < r \leqslant R_c, \end{cases} \tag{56}$$

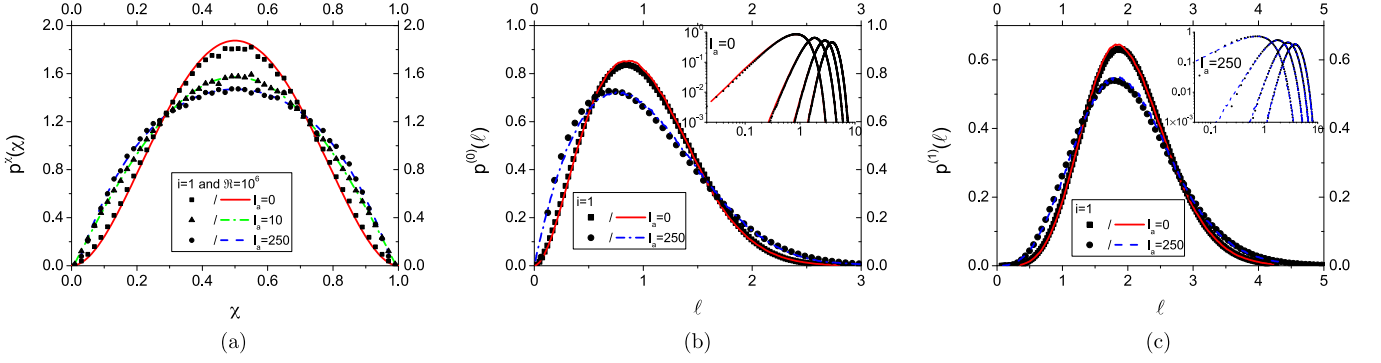FIG. 2. Case $i = 1$: (a) Fragmentation kernel $p^\chi(\chi)$, (b) gap-size distribution $p^{(0)}(\ell)$, and (c) capture-zone distribution $p^{(1)}(\ell)$ for a 1D system. The parameters used in the PM are $\ell_c = 1.7$, $\gamma_{\text{ex}} = 4$ for $l_a = 0$; and $\ell_c = 1.75$, $\gamma_{\text{ex}} = 3$ for $l_a = 250$. For $l_a = 10$, $p^{(0)}(\ell)$ and $p^{(1)}(\ell)$ (not shown) differ little from those for $l_a = 250$. The insets give log-log plots of the first four spacing distributions.

where $0 < \kappa < 1$ is a constant, and $R_c = (\mathcal{A}/\pi)^{1/2}$ is the average [scaled] radius of the CZ.

Note that in this fragmentation model, the probability to put a new center inside a cell depends only on the cell itself, regardless of the positions of neighboring centers or the areas of their surrounding cells. The simplest case corresponds to $\phi = 1$, $\delta = 0$, and $\kappa = 1$. These parameters imply $q^r(\mathbf{r}, \mathcal{A}) \propto 1/\mathcal{A}$; thus, every empty point of the lattice has the same probability to receive a new center. It is well accepted that, in this case of homogeneous nucleation, the CZ can be well described by the γ distribution [66]:

$$P(\mathcal{A}) \approx \frac{\alpha^\alpha}{\Gamma(\alpha)} \mathcal{A}^{\alpha-1} e^{-\alpha \mathcal{A}}, \tag{57}$$

where $\alpha = 7/2$ (in 2D). This framework has been used to describe the CZD for several systems [65].

Previous work (see Ref. [65]) has shown that the power δ controls the small-$\mathcal{A}$ behavior of the CZD $P(\mathcal{A})$, although how this precisely occurs remains unknown. In Ref. [65], analysis of the DLA ($l_a = 0$) regime led to the conjecture that $\delta = 1$ for critical nucleus size $i = 1$. Here we extend the conjecture to $\delta = i$ for $i > 1$, testing it with numerical simulations. In contrast, for large barriers nucleation occurs at random positions and the CZ distribution should be the same as for a Poisson point process, i.e., $P(\mathcal{A})$ is given by Eq. (57). As mentioned before, this implies $\phi = 1$ and $\delta = 0$ regardless of the value of i. Consequently, we can neglect the spatial dependence on the density, i.e., $n_1(r) \approx n$ with n a constant. Thus, the probability of a nucleation inside a particular CZ depends only on its size because $q^c(\mathcal{A}) \sim \int dr \, r \, n_1^{i+1} \sim \mathcal{A} \Rightarrow \phi = 1$. Additionally, the probability to have nucleation at a distance r from the center is the same for all points inside the CZ, so that $\delta = 0$.

For zero and weak barriers in the aggregation regime, numerical evidence suggests $1.5 \leqslant \phi \leqslant 2$ for all values of i; see the insets in Fig. 5 and more details in Refs. [62,64].

In Ref. [65], for zero barriers it was proposed $\delta = 1$ for $i = 1$ because $n_1(r)$ grows linearly close to stable islands. For general i, we propose $\delta = i$. As far as we know, the relation between δ and ζ in $P(\mathcal{A}) \sim \mathcal{A}^\zeta$ remains unknown; however, it is clear that δ controls the small-$\mathcal{A}$ tail of the CZD.

V. RESULTS

A. CZD and GSD for 1D

Now we show several examples illustrating our phenomenological approach. In the numerical simulations we use $D/F = 5 \times 10^6$ and $\theta = 0.25$. First, consider the cases with $i = 1$. For $l_a = 0$, according to the CP method $\gamma_{\text{ex}} = 4$ (see Table III), and we found empirically $\ell_c = 1.7$; the results are shown in Fig. 2. As shown in Fig. 2(a), in this case a barrier with $l_a = 10$ is strong enough to change considerably the fragmentation kernel $p^\chi(\chi)$ compared with the case of zero barrier. Consequently, the attachment barrier also changes the functional form of $p^{(0)}(\ell)$ and $P(\ell)$ (not shown). Next we consider $i = 1$ with a strong barrier $l_a = 250$. Consequently, $\gamma_{\text{ex}} = 3$ and we found $\ell_c = 2.65$. The comparison between the PM and the numerical simulation is shown in Fig. 2. The insets show the first four spacing distributions in log-log plots. The PM describes the tails of the distributions.

Figures 3 and 4 show the results for $i = 2$ and 3, respectively. In all cases, the agreement between numerical results for $p^\chi(\chi)$, $p^{(0)}(\ell)$, and $P(\ell)$ and the ones given by the PM is good. Even higher spacing distributions are well fitted by our model (see insets). Figures 3(a) and 4(a) show the numerical results for the fragmentation kernel, $p^\chi(\chi)$, for $i = 2$ and 3. In both cases, the numerical data are also well fitted by Eq. (52) and arbitrary l_a. Additionally, for $l_a = 0$ the MF approach for $p^\chi(\chi)$ becomes a better approximation as i increases.

For zero barriers, we found $\gamma_{\text{ex}} = 4$, $\gamma_{\text{ex}} = 5$, and $\gamma_{\text{ex}} = 7$ for $i = 1$, 2, and 3, respectively. These exponents are in agreement with the ones reported in Ref. [43], where $4.130 < \gamma_{\text{ex}} < 4.383$, $5.364 < \gamma_{\text{ex}} < 6.112$, and $6.094 < \gamma_{\text{ex}} < 7.437$ for $i = 1$, 2, and 3, respectively. However, the exponents for $i = 2$ and 3 used in the PM are different from the ones given by CP's approach. This is not an unexpected result: as mentioned earlier, the assumption that $n_1(x, \mathcal{L})$ has reached the stationary state at the time of the $(i + 1)$th deposition is not true for large gaps. The failure of this assumption is more pronounced as i increases. For large gaps $\omega(\mathcal{L}) \propto \mathcal{L}^{\tilde{\gamma}}$ with $\tilde{\gamma}$ an exponent which increases with i, i.e., the higher the exponent the larger the difference between nucleation rates of large and small gaps. For a given coverage ($\theta = 0.25$ in Figs. 2 to 4) the density of islands decreases as i increases. For instance, $N(0.25)$ is about 0.1, 0.03, and 0.01 for $i = 1$, 2, and 3, respectively. Then, the
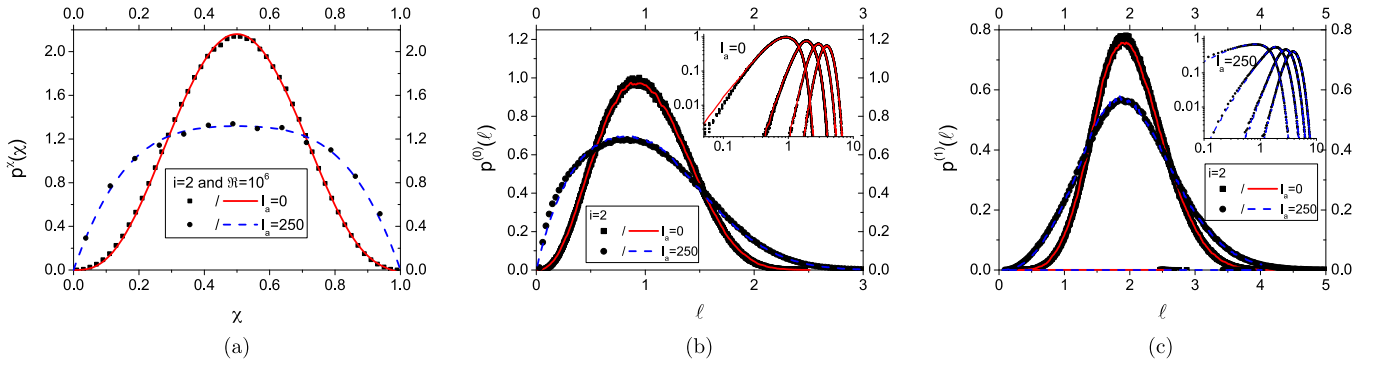
FIG. 3. Case $i = 2$: (a) Fragmentation kernel $p^\chi(\chi)$, (b) gap-size distribution $p^{(0)}(\ell)$, and (c) capture-zone distribution $p^{(1)}(\ell)$ for a 1D system. The parameters used in the PM are $\ell_c = 1.5$, $\gamma_{\rm ex} = 5$ for $l_a = 0$; and $\ell_c = 1.2$, $\gamma_{\rm ex} = 4$ for $l_a = 250$. As in Fig. 2, the insets give log-log plots of the first four spacing distributions.

average gap length is ten times as large for $i = 3$ as that for $i = 1$. Thus, we can expect that the CP approach gives good results for $i = 1$ but fails for $i = 2$ or 3 due the large average gap length.

For a given value of i and large values of l_a, the exponent $\gamma_{\rm ex}$ decreases and $p^\chi(\chi)$ becomes flatter, i.e., the nucleation events are more uniformly distributed along the gap. For zero and weak barriers, the absorbing boundaries decrease the probability of finding particles near gap edges compared with lattice sites near the middle of the gap. Consequently, the probability of nucleation near gap edges also decreases, so that its maximum value is at the middle of the gap. In the case of strong barriers, the density of particles is practically flat because the monomers need many attempts before being incorporated into an island. Consequently, the probability of $i + 1$ monomers encountering each other is practically the same for all lattice sites, i.e., nucleation events are more uniformly distributed than in the case of weak barriers. Furthermore, $p^\chi(0) = p^\chi(1) = 0$ for all finite values of l_a. This result is reproduced by the CP approach but not by MF, which predicts $p^\chi(0) = p^\chi(1) \neq 0$ for $l_a > 0$.

B. CZD for 2D

Consider first the case of weak barriers. From our numerical experimentation we estimate $\kappa = 0.3$ for $i = 1$ and $\kappa = 0.8$ for $i = 2$. For both values of i we have used $\phi = 2$. We take

$\delta = 1$ for $i = 1$ and $\delta = 2$ for $i = 2$. In this way, the nucleation probability inside a capture zone grows (linearly for $i = 1$ and quadratically for $i = 2$) with r for points near the island, while it becomes constant for points far away. As mentioned before, we can expect that these parameters also describe the CZ distribution for strong barriers and times longer than τ_a. For strong barriers in the crossover regime, the density of monomers becomes almost constant for all values of i, implying $\delta = 0$ and $\phi = 1$.

Figure 5 shows the comparison between the results of kMC simulations and the fragmentation model for $i = 1$ and $i = 2$. There is good agreement for both values of i in the cases of zero and strong barriers in the aggregation and crossover regimes, respectively. Note that, at least for $i = 1$ and $i = 2$, strong barriers imply that $P(\mathcal{A})$ can be approximated by Eq. (57), suggesting that $n_1(r)$ can be taken as a constant independent of r for the crossover regime.

VI. CONCLUSIONS

The phenomenological model we presented is quite general and simple but retains the most relevant physical properties of the 1D and 2D systems. In both cases and for arbitrary i and l_a, the structure generated by the point islands can apparently be described in terms of two different probabilities which describe the nucleation process inside a gap for 1D and inside a capture zone for 2D. Furthermore, by describing the nucleation in
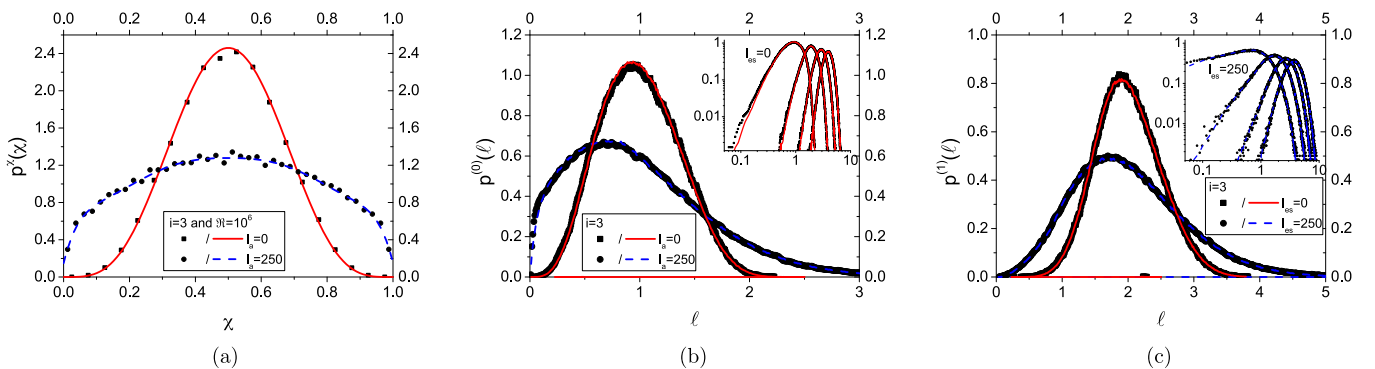

FIG. 4. Case $i = 3$: (a) Fragmentation kernel $p^\chi(\chi)$, (b) gap-size distribution $p^{(0)}(\ell)$, and (c) capture-zone distribution $p^{(1)}(\ell)$ for a 1D system. The parameters used in the PM are $\ell_c = 1.5$, $\gamma_{\rm ex} = 7$ for $l_a = 0$; and $\ell_c = 1.0$, $\gamma_{\rm ex} = 3$ for $l_a = 250$. As in Fig. 2, the insets give log-log plots of the first four spacing distributions.
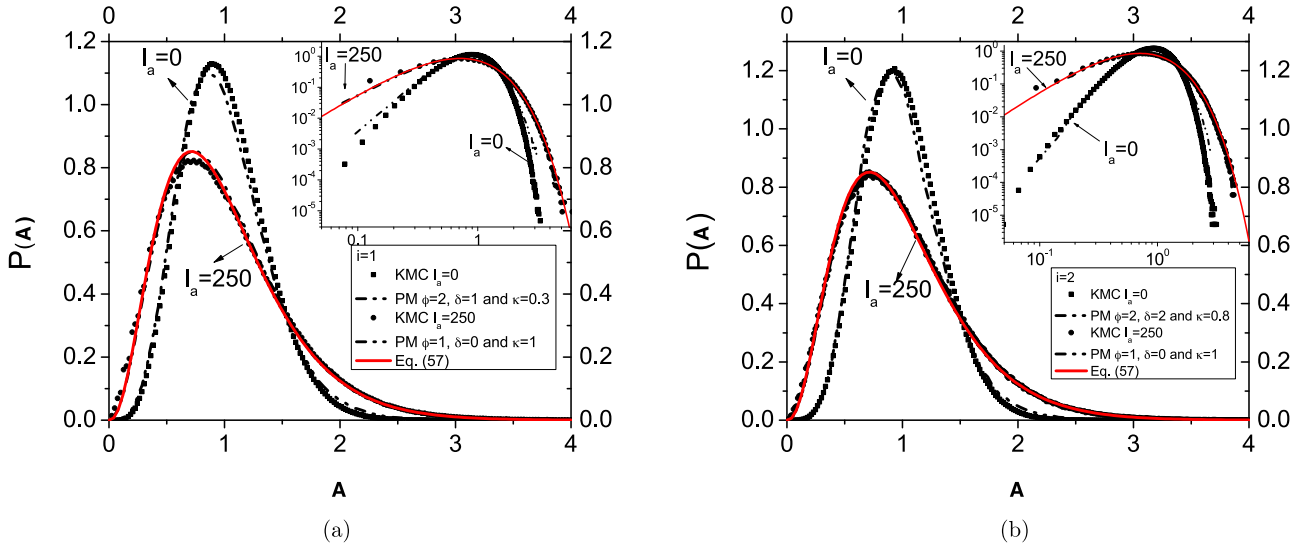
FIG. 5. Capture zone distributions for kMC simulations in 2D (dense discrete symbols) with (a) $i = 1$ and (b) $i = 2$ with $l_a = 0$ (narrower set of curves) and $l_a = 250$ (broader set). In all cases, the fragmentation (PM) approach (dash-dotted curves) gives excellent results. The insets show log-log plots of the kMC results for $P(\mathcal{A})$. Note that Eq. (57), kMC results for $l_a = 250$ and the PM with $\phi = 1$, $\delta = 0$, and $\kappa = 1$ are almost indistinguishable for both i values.

conjunction with an appropriate fragmentation model, we can find the growth exponents and the CZD or GSD. Since the CZD is usually measurable experimentally, we can use it to actually calculate microscopic parameters of the model such as i and l_a.

Specifically, in 1D the mean nucleation probability density $p^\chi(\chi)$ and the gap-size-dependent nucleation rate $\omega(\mathcal{L})$ are enough to understand the nucleation process. For small values of l_a, most of the nucleation events occur near the middle of the gap, and $p^\chi(\chi)$ has a well-defined maximum. For large values of l_a the nucleation events are more homogeneously distributed along the gap, and $p^\chi(\chi)$ is almost flat near the middle of the gap. For all values of l_a and i, $p^\chi(0) = 0 = p^\chi(1)$, implying that the density of monomers changes quickly near stable islands.

Additionally, $p^{(0)}(\ell) \propto \ell^\mu$ for $\ell \to 0$ where μ is given by the MF theory for weak barriers [$\mu = 2(i + 1)$], while for large barriers $\mu < 1$, so that the GSD changes quickly for small values of ℓ. Assuming that the CZD can be written as the convolution product of two GSDs, the behavior of the CZD for small ℓ is given by $P(\ell) \propto \ell^{2\mu+1}$. The CP approach gives "exact" results for $\omega(\mathcal{L})$ and $p^\chi(\chi)$, but some corrections are necessary, mainly because of the assumption—untrue for large gaps—that when the $(i + 1)$th monomer arrives, the density of monomers has achieved its stationary state. MF describes $p^\chi(\chi)$ well for zero and weak barriers. Table III shows the exact values of γ_{ex} for different values of i; in general we found good agreement with numerical data taking the nucleation-rate exponent $\gamma = \gamma_{\mathrm{ex}} - 1$ for $\ell > \ell_c$.

Despite its implicit simplifications (such as homogeneity and isotropy), our model proves to be a powerful tool to describe CZDs in 2D. The effect of the attachment barrier is included through the density of monomers inside a CZ, $n(r)$. For the 2D case and arbitrary i, large barriers imply that for the crossover regime there is a homogeneous distribution of monomers inside the CZ, which leads to the case where the

position of the islands are not correlated: $\delta = 0$ and $\phi = 1$. Consequently, for large barriers in the crossover regime, $P(\mathcal{A})$ is independent of the value of i. For large times the DLA regime is recovered. The attachment barrier is reflected in the exponents γ, δ and in the constant κ used in our fragmentation model. For weak barriers in the aggregation regime, $\delta = i$. For strong barriers in the crossover regime, $\delta = 0$. The value of ϕ is near 2 for weak barriers and for strong barriers in the aggregation regime, but for strong barriers in the crossover regime $\phi = 1$.

APPENDIX: GENERAL RATE EQUATIONS

In the point-island model, the time evolution of the densities of free monomers, N_1, and of islands containing n monomers, N_n, is given by the rate equations [23,27,46]

$$\frac{dN_1}{d\theta} = (1 - N) - (i + 1)N_i - (i + 1)\sigma_u \frac{D}{F} N_1 N_i$$
$$- \frac{D}{F} N_1 \sum_{n \geqslant i+1} \sigma_n N_n, \tag{A1}$$

$$\frac{dN_n}{d\theta} = \frac{D}{F} N_1(\sigma_{n-1} N_{n-1} - \sigma_n N_n) + N_{n-1} - N_n, \tag{A2}$$

respectively. The fraction of the substrate that is not covered by stable islands is $1 - N$. The second term of Eq. (A1) and

the last two terms of Eq. (A2) represent the direct deposition of monomers on top of islands with sizes i, $n-1$, and n, respectively. The formation of new islands is represented by the third and the first terms of Eqs. (A1) and (A2), respectively. Finally, the last term of Eq. (A1) represents the aggregation of monomers to stable islands. Since we are interested on the evolution of the total density of islands, the sum over $n > i$ is performed on Eq. (A2). Consequently,

$$\frac{dN}{d\theta} = \frac{D}{F} N_1 \sigma_i \ N_i + N_i. \tag{A3}$$

In our simulation, monomers are deposited only on empty sites. Thus, the second term of Eq. (A1) and the last one of Eq. (A3) can be neglected. Finally, because of our assumption that bonding energies vanish inside unstable islands, Walton's relation [58] reads $N_i = N_1^i$. After some algebra, and using the definition

$$\sigma_s = \frac{1}{N} \sum_{n \geqslant i+1} \sigma_n N_n \tag{A4}$$

for the capture coefficient of stable islands, it is straightforward to obtain Eqs. (2) and (3).

[1] H. J. Fecht, Europhys. News **28**, 89 (1997).

[2] R. C. Ball, D. A. Weitz, T. A. Witten, and F. Leyvraz, Phys. Rev. Lett. **58**, 274 (1987).

[3] H. Kallabis, P. L. Krapivsky, and D. E. Wolf, Eur. Phys. J. B **5**, 801 (1998).

[4] P. Meakin and F. Family, Phys. Rev. A **38**, 2110 (1988).

[5] Z. Zhang and M. G. Lagally, Science **276**, 377 (1997).

[6] T.-C. Chang, I.-S. Hwang, and T. T. Tsong, Phys. Rev. Lett. **83**, 1191 (1999).

[7] T.-C. Chang, K. Chatterjee, S.-H. Chang, Y.-H. Lee, and I.-S. Hwang, Surf. Sci. **605**, 1249 (2011).

[8] I.-S. Hwang, T. C. Chang, and T. T. Tsong, Phys. Rev. Lett. **80**, 4229 (1998).

[9] I.-S. Hwang, T. C. Chang, and T. T. Tsong, Jpn. J. Appl. Phys. **39**, 4100 (2000).

[10] E. Loginova, N. C. Bartelt, P. J. Feibelman, and K. F. McCarty, New J. Phys. **10**, 093026 (2008).

[11] E. Loginova, N. C. Bartelt, P. J. Feibelman, and K. F. McCarty, New J. Phys. **11**, 063046 (2009).

[12] H. S. Mok, A. Ebnonnasir, Y. Murata, S. Nie, K. F. McCarty, C. V. Ciobanu, and S. Kodambaka, Appl. Phys. Lett. **104**, 101606 (2014).

[13] J. Ning, D. Wang, D. Han, Y. Shi, W. Cai, J. Zhang, and Y. Hao, J. Cryst. Growth **424**, 55 (2015).

[14] J. Park, J. Lee, J.-H. Choi, D. K. Hwang, and Y.-W. Song, Sci. Rept. **5**, 11839 (2015).

[15] C. Ratsch and J. A. Venables, J. Vac. Sci. Technol. A **21**, S96 (2003).

[16] H. Jónsson, Annu. Rev. Phys. Chem. **51**, 623 (2000).

[17] S. M. Binz, M. Hupalo, X. Liu, C. Z. Wang, W.-C. Lu, P. A. Thiel, K. M. Ho, E. H. Conrad, and M. C. Tringides, Phys. Rev. Lett. **109**, 026103 (2012).

[18] P. Meakin, in *Phase Transitions and Critical Phenomena*, edited by C. Domb and J. L. Lebowitz (Academic Press, New York, 1988), Vol. 12, p. 335.

[19] R. Jullien and M. Kolb, J. Phys. A **17**, L639 (1984).

[20] L. Tumbek and A. Winkler, Surf. Sci. **606**, L55 (2012).

[21] A. Pimpinelli, L. Tumbek, and A. Winkler, J. Phys. Chem. Lett. **5**, 995 (2014).

[22] J. R. Morales-Cifuentes, T. L. Einstein, and A. Pimpinelli, Phys. Rev. Lett. **113**, 246101 (2014).

[23] J. A. Blackman and P. A. Mulheran, Phys. Rev. B **54**, 11681 (1996).

[24] J. G. Amar, F. Family, and P.-M. Lam, Phys. Rev. B **50**, 8781 (1994).

[25] D. Kandel, Phys. Rev. Lett. **78**, 499 (1997).

[26] C. Ratsch, A. Zangwill, P. Šmilauer, and D. D. Vvedensky, Phys. Rev. Lett. **72**, 3194 (1994).

[27] J. A. Venables, G. D. Spiller, and M. Hanbucken, Rep. Prog. Phys. **47**, 399 (1984).

[28] J. W. Evans, P. A. Thiel, and M. C. Bartelt, Surf. Sci. Rep. **61**, 1 (2006).

[29] B. Müller, L. Nedelmann, B. Fischer, H. Brune, and K. Kern, Surf. Diffusion **360**, 151 (1997).

[30] H. Brune, H. Röder, C. Boragno, and K. Kern, Phys. Rev. Lett. **73**, 1955 (1994)

[31] J. A. Stroscio and D. T. Pierce, Phys. Rev. B **49**, 8522 (1994).

[32] J. K. Zuo, J. F. Wendelken, H. Dürr, and C.-L. Liu, Phys. Rev. Lett. **72**, 3064 (1994).

[33] M. C. Bartelt and J. W. Evans, Phys. Rev. B **46**, 12675 (1992).

[34] M. C. Bartelt and J. W. Evans, Phys. Rev. B **54**, R17359(R) (1996).

[35] F. Shi, Y. Shim, and J. G. Amar, Phys. Rev. E **79**, 011602 (2009).

[36] Y. Han, É. Gaudry, T. J. Oliveira, and J. W. Evans, J. Chem. Phys. **145**, 211904 (2016).

[37] T. L. Einstein, A. Pimpinelli, and D. L. González, J. Cryst. Growth **401**, 67 (2014); T. L. Einstein, A. Pimpinelli, D. L. González, and J. R. Morales-Cifuentes, J. Phys.: Conf. Ser. **640**, 012024 (2015).

[38] Y. Han and M. Li, and J. W. Evans, J. Chem. Phys. **145**, 211911 (2016).

[39] A. Pimpinelli and T. L. Einstein, Phys. Rev. Lett. **99**, 226102 (2007).

[40] A. Pimpinelli and T. L. Einstein, Phys. Rev. Lett. **104**, 149602 (2010).

[41] P. Gambardella, H. Brune, K. Kern, and V. I. Marchenko, Phys. Rev. B **73**, 245425 (2006).

[42] D. L. González, A. Pimpinelli, and T. L. Einstein, Phys. Rev. E **84**, 011601 (2011).

[43] K. P. O'Neill, M. Grinfeld, W. Lamb, and P. A. Mulheran, Phys. Rev. E **85**, 021601 (2012).

[44] J. G. Amar and F. Family, Thin Solid Films **272**, 208 (1996).

[45] J. G. Amar and M. N. Popescu, Phys. Rev. B **69**, 033401 (2004).

[46] J. G. Amar, M. N. Popescu, and F. Family, Surf. Sci. **491**, 239 (2001).

[47] A. Chame and F. D. A. Aarão Reis, Phys. A **376**, 108 (2007).

[48] P. P. Petrov, W. Miller, U. Rehse, and R. Fornari, Appl. Math. Model. **35**, 1331 (2011).

[49] R. B. Stinchcombe and F. D. A. Aarão Reis, Phys. Rev. B **77**, 035406 (2008).

[50] P. Politi and J. Villain, Phys. Rev. B **54**, 5114 (1996).

[51] D. L. González, J. Phys. A: Math. Theor. **50**, 035001 (2017).

[52] J. Krug, P. Politi, and T. Michely, Phys. Rev. B **61**, 14037 (2000).

[53] D. L. González, Revista de Ciencias **18**, 81 (2014).

[54] R. P. Treat, J. Phys. A: Math. Gen. **30**, 2519 (1997).

[55] Z. Cheng and S. Redner, Phys. Rev. Lett. **60**, 2450 (1988).

[56] M. Grinfeld, W. Lamb, K. P. O'Neill, and P. A. Mulheran, J. Phys. A: Math. Theor. **45**, 015002 (2012).

[57] P. A. Mulheran, K. P. O'Neill, M. Grinfeld, and W. Lamb, Phys. Rev. E **86**, 051606 (2012).

[58] D. Walton, J. Chem. Phys. **37**, 2182 (1962).

[59] C. Castellano and P. Politi, Phys. Rev. Lett. **87**, 056102 (2001).

[60] P. Politi and C. Castellano, Phys. Rev. E **66**, 031605 (2002).

[61] P. Politi and C. Castellano, Phys. Rev. E **66**, 031606 (2002).

[62] M. Li, Y. Han, and J. W. Evans, Phys. Rev. Lett. **104**, 149601 (2010).

[63] T. J. Oliveira and F. D. A. Aarão Reis, Phys. Rev. B **83**, 201405(R) (2011).

[64] T. J. Oliveira and F. D. A. Aarão Reis, Phys. Rev. B **86**, 115402 (2012).

[65] D. L. González and T. L. Einstein, Phys. Rev. E **84**, 051135 (2011).

[66] J.-S. Ferenc and Z. Néda, Physica A **385**, 518 (2007).